

Observational Properties of Near-Maximal Spin Black Holes with the EHT

Tegan A. Thomas^{1,2,3*} , Angelo Ricarte^{4,5} , Ben S. Prather⁶ , Hyerin Cho^{4,5} , and Yajie Yuan¹ 
Advisors: Angelo Ricarte^{4,5} & Yajie Yuan¹

¹Department of Physics, Washington University in St. Louis, 1 Brookings Dr, St. Louis 63130, United States

²Smithsonian Astrophysical Observatory,

³National Society of Black Physicists,

⁴Black Hole Initiative, Another Institution, Street Address, City Postal Code, Country

⁵Center for Astrophysics, Harvard University & Smithsonian,

⁶Los Alamos National Laboratory

ABSTRACT

In 2021 and 2024 the Event Horizon Telescope (EHT) collaboration published the first polarized images of the supermassive black holes (SMBHs) M87* and Sgr A*, which allowed us to place important constraints on the accretion flow and underlying space-time. Of particular interest is the dimensionless spin parameter " a_* ", which theoretically may attain a maximum value of $a=0.998$ when spun up by a thin accretion disk. On the other hand, mechanisms including incoherent accretion, SMBH mergers, and spin extraction via jets, are hypothesized to spin down SMBHs from these near-extremal values. In this work, we perform general relativistic magnetohydrodynamics (GRMHD) simulations of $a=0.998$ SMBHs with advection-dominated and strongly magnetized accretion disks to determine their observational characteristics. First, we evolve the fluid in a Kerr space-time to study properties, including its variability, magnetic flux accumulated on the horizon, and jet power. Then, we perform general relativistic ray-tracing (GRRT) to produce polarized movies that can be directly compared to current and future EHT observations. We predict increased jet power efficiency as well as distortions to the photon ring which should be an accessible signature that extensions to the EHT, such as the next-generation EHT (ngEHT) and Black Hole Explorer (BHEX), can then use to rule out such models.

NOTE: THIS IS A DRAFT VERSION

1. INTRODUCTION

In 2019 the Event Horizon Telescope (EHT) collaboration successfully created the first image of a black hole with the picture of M87 [1]. This was then followed up with the image of the black hole at the center of the Milky Way, Sgr A* in 2022 [2]. These images have allowed us to gain incredible insight into the physics happening around supermassive black holes (SMBHs), as it serves as a source of data which may be compared against black hole models. The corresponding EHT polarized observation of M87* in 2021 and Sgr A* in 2024 helped map out the polarization structure of these sources, enhancing our models of near-horizon magnetic fields— a key probe of black hole spin [3, 4].

Moving forward, the next-generation Event Horizon Telescope (ngEHT) will improve upon EHT by adding more radio dishes to the Very Long Baseline Interferometric (VLBI) array and observing at 3 frequencies simultaneously (?) [5]. This will result in better resolution and spatial frequency coverage for observations of M87 and Sgr A* (?) [5]. Additionally, the proposed BHEX mission would further expand the EHT into space, vastly improving our resolution to the order of $5\mu\text{as}$ (?) [6]. With BHEX, we could begin to image

other SMBHs besides Sgr A* and M87*, further increasing the importance of having methods with which we may constrain black hole parameters such as inclination or magnetic field strength (?) [6].

One of the key parameters in this context is the dimensionless spin parameter a_\bullet , as defined by the equation below where J is the angular momentum and M_{BH} is the black hole mass [7]. Especially when looking at event horizon scale observations, a_\bullet is critical as it significantly impacts evolution and dynamics of the nearby disk.

$$a_\bullet = \frac{cJ}{GM_{BH}^2} \quad (1)$$

a_\bullet is measured between -1 and 1, however due to radiation the upper limit of a black hole's spin is 0.998 for black holes with a thin accretion disk [8]. Additionally, it has been shown that black holes do not always reach this maximum spin of 0.998 and can instead reach equilibrium at lower spins [9–14].

In addition to impacting the dynamics of the accretion disk, spin also has cosmological importance. For instance, the spin distribution of black holes in the universe can indicate the role of different types of accretion episodes [15] or informing theories of how jet feedback impacts spin [12]. Multiple proposed methods of spin evolution have even found that, theoretically, there should be nearly no maximally spinning black holes [15]. Therefore observing a maximally spinning black hole, or being able to rule out a significant number of black holes as not maximally spinning, would help narrow our options for spin evolution mechanisms and would have significant cosmological implications.

In order to observe such an object, we must first know what near-maximal spin SMBHs should look like. As spin approaches 1, many black hole properties evolve rapidly, potentially resulting in unique observational characteristics and rapid evolution over spin. Our project aims to identify observational characteristics of near-maximal spin black holes and probe evolution over spin by presenting one of the first polarized movies of $a_\bullet = 0.998$ SMBHs and comparing it to $a_\bullet = 0.9375$ counterparts.

In section 3 we will discuss the code used, specifically KHARMA for GRMHD and IPOLE for GRRT. Additionally, we will explain the units used and potential limitations to the simulations. Then in section 4 we will go over the initial results found before reviewing our results and analyzing the implications for potential EHT observations of maximally spinning black holes in section 5.

2. THEORY OF KERR BLACK HOLES AND THEIR OBSERVABLES

2.1. Jet Luminosity

The Blandford-Znajek mechanism is a key model that links relativistic jet power to black hole spin [16].

The model suggests that, due to the spin of BH, the magnetic field that threads the black hole is twisted into coils, forming a large toroidal field component along the jet. This toroidal field then exerts an upward magnetic pressure on the surrounding plasma, and this pressure builds over time. Eventually, in order to maintain stability, the plasma pressure must decrease and so plasma is accelerated upwards, creating a jet. [16, 17]

This process is best demonstrated with the diagram below [17].

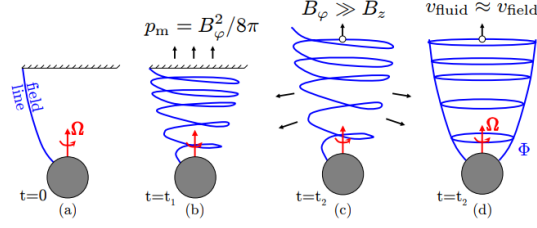


Figure 1. Above is a diagram from Davis & Tchekhovskoy (2021) demonstrating the BZ mechanism [17]. As a black hole spins it twists the initially poloidal magnetic fields, producing a toroidal component. This component builds up, becoming a "magnetic spring" of sorts and eventually it is large enough to push away a layer of plasma and it begins to continually accelerate plasma upwards. Eventually the magnetic field can be estimated as primarily toroidal, at which point the plasma acceleration is mainly driven by the established pressure gradient.

Since the jet is driven by the dragging of the magnetic fields it makes sense that, for slowly spinning black holes ($a_{\bullet} \ll 1$), the jet luminosity relates to magnetic flux onto the horizon (Φ_B) and spin (a_{\bullet}) via the equation below.

$$L_{BZ} \propto a_{\bullet}^2 \Phi_B^2 \quad (2)$$

As the spin approaches one, the jet becomes more luminous and powerful, extracting increased amount of energy from the black hole. This is evaluated using the jet power efficiency, defined below.

$$\eta = \frac{P_{jet}}{\langle \dot{M}_0 \rangle c^2} \quad (3)$$

In this paper, "accretion rate", \dot{M}_0 , specifically refers to the rest mass inflow rate through the disk, not necessarily the net rate of change of the black hole rest mass [18].

For MAD black holes Narayan et al. (2022) finds that this jet power efficiency increases with increased spin in such a way that agrees with the predicted relationship found in Tchekhovskoy et al. (2010) written below [11, 19].

$$\eta_{BZ6} = \frac{\kappa}{4\pi} \phi_{BH}^2 \Omega_H^2 [1 + 1.38\Omega_H^2 - 9.2\Omega_H^4] \quad (4)$$

where $\Omega_H = \frac{a_{\bullet}}{2r_H}$. Specifically, Narayan et al. (2022) found agreement between their findings and Tchekovskoy's equation for $\kappa = 0.05$, where κ is a constant whose precise value is determined by the initial field geometry [11]. We expect that for the near-maximal spin case this jet power efficiency should continue to increase even beyond 1, implying that more energy is extracted via the jet than produced from accretion. Such behavior was observed for MAD models with a spin of 0.9, but should be more extreme for the near-maximal spin of 0.998.

For systems with sufficiently high magnetic field, the angular momentum and energy loss from these powerful jets may exceed the momentum gained from the disk, resulting in the black hole spinning down [11]. The spin-up of a black hole is analyzed using the dimensionless spin up parameter s as defined below where a negative value indicates spin down [9, 10, 18].

$$s = \frac{d(J/M^2)}{dt} \frac{M_{BH}}{\dot{M}_0} = \frac{da_{\bullet}}{dt} \frac{M_{BH}}{\dot{M}_0} \quad (5)$$

As the spin increases, this spin up parameter should become increasingly negative indicating intense spin down of the black hole [11]. In this way, jets heavily influence the spin evolution of black holes.

Jet power is also important because of the role jets play in galaxy evolution. Jets insert large amounts of energy within their host galaxies over very long distances which heats galaxy halos and prevents gas from

cooling, potentially limiting star formation. The heated gas also is more broadly distributed and less dense, resulting in decreased accretion and therefore decreased jet power. This cycle of influence between jets and their host galaxies is known as jet-driven AGN feedback and is a blossoming area of research as the exact mechanisms and impacts of large jet power are still being determined.

It is through AGN feedback as well as BH spin evolution that our findings on jet power efficiency for near-maximal black holes can have important implications about galaxy evolution as a whole.

2.2. Accretion Flow Properties

Besides the impact on jets, the spin of a black hole also directly impacts the position of the event horizon, which in turn also influences accretion flow.

The event horizon is defined as the surface along which the escape velocity is the speed of light. The equation for the event horizon radius is below.

$$r_{EH} = \frac{GM_{BH}}{c^2} [1 + \sqrt{1 - a_*^2}] \quad (6)$$

As spin increases, the event horizon shrinks allowing us to probe the area closer to the black hole. While the emission from nearby the event horizon is significantly redshifted, it still constitutes a notable portion of our observed emission which is known as the "inner shadow" [20]. This inner shadow appears as a brightness depression, the edge of which is a lensed image of the event horizon [20]. Being able to observe and identify such a feature would not only directly allow us to probe black hole spin, since the EH radius is directly related to spin, but also would help indicate accretion disk & jet geometry as the inner shadow only appears in the case that emission is concentrated to the equatorial plane [20].

The event horizon more directly influences accretion flow because, as one approaches closer to the singularity, more efficient energy extraction becomes possible. With a smaller event horizon then, this extra energy and radiation can meaningfully impact the rest of the accretion disk by heating it up. This can even be seen within previous models, where it was generally noted that accretion disk temperature tended to increase with increasing spin [21].

2.3. Photon Ring

The Event Horizon Telescope is able to image black holes on event horizon scales because not all of the emission from the accretion disk around a black hole falls into the black hole. Instead some of the light is lensed by the black hole's intense gravity and eventually makes its way to Earth, which is what we see when we get a picture of a black hole.

Out of this light that we end up seeing, most of it was emitted and directly lensed in our direction. However, the gravitational lensing of the black hole is powerful enough that some light orbits the black hole before going in our direction, creating a fainter ring of light within our final image which we call the photon ring.

Within the photon ring there are sub-rings that are indexed by n , where each photon within that sub-ring has performed $[n+1, n+2)$ half-orbits [22]. As n goes to ∞ the image approaches the "critical curve"; an image predicted by General Relativity that acts as the boundary between the geodesics that can and can't reach us [22]. This critical curve can be analytically determined by the mass, distance, spin, and viewing inclination of the black hole [22].

Given that for most black hole sources potentially resolvable to EHT the mass and distance can be

approximated using other astronomical methods or the general size of the black hole shadow, being able to resolve the critical curve would give us key information to constrain the potential combinations of spin and inclination of that black hole.

The $n=0$ ring dominates most emission, and each subsequent ring gets substantially fainter as the parameters to allow for multiple orbits become more specific, making perfect imaging of the critical curve difficult. However, the rings get closer to the critical curve exponentially so the $n=1$ and sometimes $n=2$ rings are very promising as they are the most feasible to potentially resolve and still give great insight into the potential spin and inclination of a black hole. Efforts are being made to potentially resolve the photon ring of M87 or Sgr A* using the ngEHT and the Black Hole Explorer (BHEX) in the future [6].

Looking at spin specifically, the critical curve changes in diameter, position, and shape as spin increases. These changes are also dependant on the inclination and typically edge-on inclination allows for the most noticeable photon ring differences as shown below.

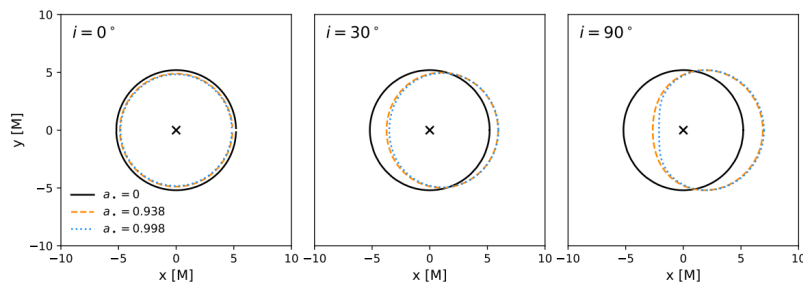


Figure 2. The analytically determined critical curve for spins of $a_{\bullet} = 0, 0.9375,$ and 0.998 is shown for inclinations of $0^{\circ}, 30^{\circ},$ and 90° . The code to make this image is from Ricarte et al. 2023 [23], and is based on equations from Chael et al. 2021 [24].

The figure demonstrates how at 0° inclination the primary effect is on the decreasing radius of the critical curve for increasing spin, meanwhile for 30° a translational shift becomes noticeable, and at 90° the shape of the curve is impacted as it flattens on the left-hand side with increasing spin.

3. METHODOLOGY

3.1. GRMHD Simulations

For our GRMHD simulations, we followed the framework outlined in Wong et al. 2022 [25].

In order to model the plasma around black holes we use the General Relativistic Magneto-Hydrodynamic (GRMHD) code known as KHARMA. KHARMA works by utilizing Parthenon to track the density (ρ), internal energy (u), four-velocity (\tilde{u}^i), and magnetic field (B^i) of the plasma as it travels between cells [25]. These are known as our "primitive variables" and they are used to compute conserved quantities such as the stress energy tensor T_{ν}^{μ} [25]. The equations which govern GRMHD and allow us to get conserved quantities from the primitives are listed below.

$$\delta_t(\sqrt{-g}\rho u^t) = -\delta_i(\sqrt{-g}\rho u^i) \quad (7)$$

$$\delta_t(\sqrt{-g}T^t_\nu) = -\delta_i(\sqrt{-g}T^i_\nu) + \sqrt{-g}T^\kappa_\lambda \Gamma^\lambda_{\nu\kappa} \quad (8)$$

$$\delta_t(\sqrt{-g}B^i) = -\delta_j[\sqrt{-g}(b^j u^i - b^i u^j)] \quad (9)$$

$$\delta_i(\sqrt{-g}B^i) = 0 \quad (10)$$

In these equations g is the determinant of the Kerr metric and Γ is the Christoffel symbol.

3.1.1. Units

Throughout this paper distance and time is expressed in terms of M , the black hole mass parameter GM_{BH}/c^2 , based on the following equations for gravitation radii and time.

$$\begin{aligned} r_g &= \frac{GM_{BH}}{c^2} = M \\ t_g &= \frac{GM_{BH}}{c^3} = \frac{r_g}{c} \end{aligned} \quad (11)$$

Most works take $G=c=1$, and so time is then also referred to in units M .

Additionally, within KHARMA we utilize a coordinate system known as "Modified Kerr-Schild" or mks. This coordinate system increases the number of grid zones around the midplane based on a parameter $hslope$, allowing for increased effective resolution within the disk.

3.1.2. Initial Conditions & Parameters

We begin each simulation with a Fishbone & Moncrief torus with an innermost radius of $r_{in} = 20M$ and a radius of maximum pressure of $r_{max} = 41M$ centered around the black hole [26]. We establish the black hole as having some spin a_\bullet and apply MAD magnetic field initial conditions to the torus. From there, the plasma begins accreting over time. We primarily focus on the results from the simulation past $t \approx 5,000M$ as beyond that point the black hole should be relatively stable and should no longer be significantly impacted by the initial torus condition.

Throughout the simulation we maintain a constant adiabatic index $\hat{\gamma}$ of $\frac{13}{9}$, which is between the expected index values of $\frac{5}{3}$ and $\frac{4}{3}$ for plasma temperatures below and above $\frac{m_e c^2}{k_b}$ respectively [27].

For these runs we focus on Magnetically Arrested Disks (MAD) where the magnetic flux upon the horizon builds via constant accretion until it becomes sufficiently large and dynamically important as the magnetic pressure counteracts the inflow [28]. By comparison, Standard and Normal Evolution (SANE) disks have a weak turbulent magnetic field which does not become dynamically important and doesn't magnetically arrest the fluid despite simulating over long time frames [29]. We decided to focus on MADs partially because they currently offer the most promising models for Sgr A* when comparing observed data to GRMHD models [21].

The near-maximal spin KHARMA run faced some difficulties with floors resulting in material being inserted along the jet, and so transmitting boundary conditions and B_ϕ reconnection was adopted. These changes make it so that magnetic loops around the pole can be connected despite being in different "zones", preventing $\nabla \cdot B$ from growing uncontrollably, and also allow for inserted material to better distribute along

the poles, preventing a large amount of material inserted on one side from building up and causing an explosion.

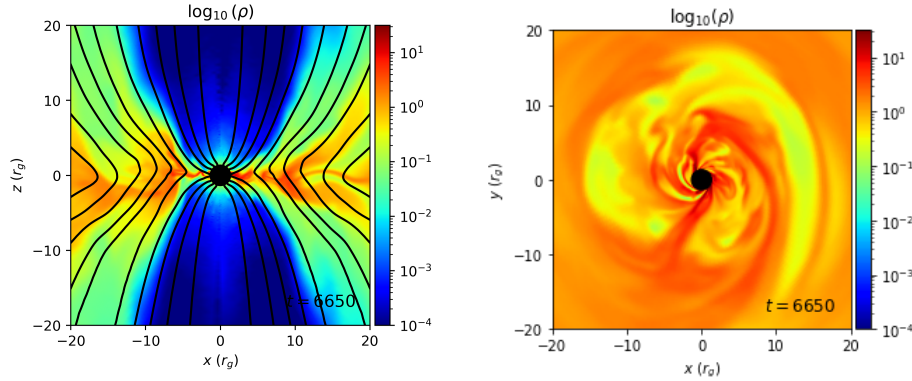


Figure 3. Above are two images showing the xz and xy slice of a typical GRMHD snapshot. The color denotes the log density and the contour lines show the poloidal magnetic field.

3.2. GRRT Imaging

In order to image the GRMHD simulations we get from KHARMA we utilize the General Relativistic Radiative Transfer (GRRT) code known as IPOLE, which is explained in more detail in Mościbrodzka & Gammie (2018)[30]. IPOLE works by first establishing a grid and information about the black hole and plasma using files from KHARMA. It then tracks the photon path from the camera towards the black hole, stopping once it hits the event horizon, goes off past a certain radius, or once a maximum number of steps has been taken. Finally, it integrates the equations of polarized radiative transfer forward towards the camera. Throughout these steps we have taken on the "fast-light" assumption where we argue that the timescale it would take for the light to travel through the accretion disk is small enough that the disk doesn't change during it, and so we can create an image from a single GRMHD file. The equations that we integrate can be found below.

$$\frac{d}{ds} \begin{pmatrix} I_v \\ Q_v \\ U_v \\ V_v \end{pmatrix} = \begin{pmatrix} j_{v,I} \\ j_{v,Q} \\ j_{v,U} \\ j_{v,V} \end{pmatrix} - \begin{pmatrix} \alpha_{v,I} & \alpha_{v,Q} & \alpha_{v,U} & \alpha_{v,V} \\ \alpha_{v,Q} & \alpha_{v,I} & \rho_{v,V} & -\rho_{v,U} \\ \alpha_{v,U} & -\rho_{v,V} & \alpha_{v,I} & \rho_{v,Q} \\ \alpha_{v,V} & \rho_{v,U} & -\rho_{v,Q} & \alpha_{v,I} \end{pmatrix} \begin{pmatrix} I_v \\ Q_v \\ U_v \\ V_v \end{pmatrix} \quad (12)$$

In this equation, I Q U & V are the Stokes parameters indicating overall intensity (I), linear polarization intensity (Q and U), and circular polarization intensity (V). The values $j_{v,-}$, where the blank is instead one of the four Stokes parameters, represent the emission coefficients, the values $\alpha_{v,-}$ represent the absorption coefficients, and the values $\rho_{v,-}$ represent the rotation coefficients. In this way, the equation shows that the change in intensities over each step is based on the amount of new emission minus the amount of absorption and rotation that acts on previous emission.

When determining emission we focus primarily on synchrotron radiation as it dominates current EHT observations. Additionally, with IPOLE we are able to get the Stokes parameters to determine the polarization of light.

With IPOLE we are able to image GRMHD simulations to incredibly high resolution, which allows for us to explore theoretical effects of certain characteristics on images. However, in order to properly compare

with EHT data we may apply a Gaussian beam to blur the image so that it is comparable to EHT’s resolution of $20\mu\text{as}$.

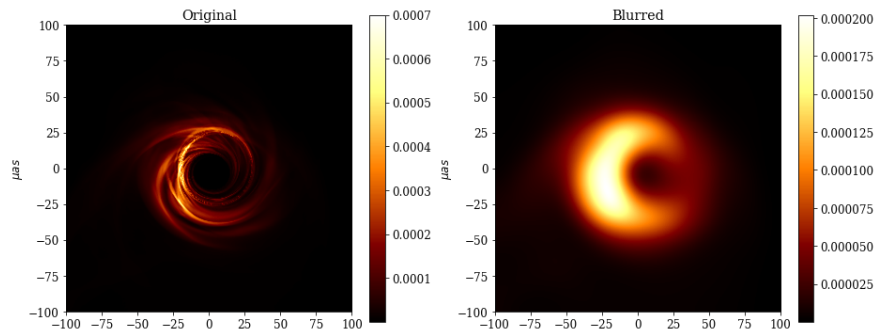


Figure 4. Above is an example of an IPOLE snapshot. On the left is the original image produced by IPOLE and then on the right is a blurred version which shows what EHT would actually observe.

Additionally, since we track the null geodesic that photons travel upon, we are able to easily decompose the photon rings, allowing us to analyze how they are impacted by maximal spin.

Making a movie via IPOLE is relatively straight forward. We image a series of GRMHD files chronologically and then are able to put the images together to make a movie. However, one caveat is that in IPOLE the variable “M_unit” is used to scale the accretion rate of the black hole to a known object’s flux, in this case we match it to Sgr A*’s flux of $\approx 2.4Jy$.

4. RESULTS

The aforementioned process was used to model and image black holes with $a_{\bullet} = 0.9375$ and $a_{\bullet} = 0.998$ and for inclinations of 150° and 90° . Our GRMHD simulations ran up till $t=10,000M$, although the first 5,000M timesteps aren’t included in these results in order to avoid any influence of initial conditions. The following results and analysis are all based on the 5,000-10,000M time window for both simulations.

4.1. Black Hole Properties

4.1.1. Accretion Rate

The accretion rate is calculated within PYHARM by looking at the mass flux (rate of mass flow per unit area) at $r = 5M \pm 0.03M$ (where the $\pm 0.03M$ is due to zone values not aligning strictly at $5M$) and is represented with the variable \dot{M} .

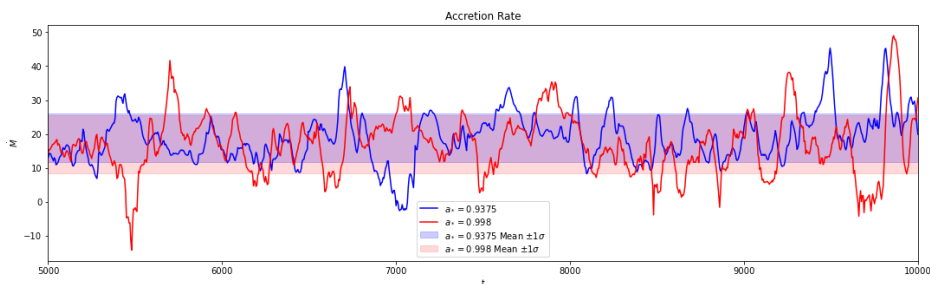


Figure 5. The accretion rate as a function of time is shown for both $a_{\bullet} = 0.9375$ (blue) and $a_{\bullet} = 0.998$ (red). The highlighted blue and red regions show the mean accretion rate $\pm 1\sigma$ for $a_{\bullet} = 0.9375$ and 0.998 respectively.

The average accretion rate for $a_{\bullet} = 0.9375$ versus $a_{\bullet} = 0.998$ looking from $t = 5,000M$ onwards is ~ 18.84 and ~ 16.97 respectively. This agrees with the graph visually showing that the average accretion rate is generally similar between the two runs, although the mean does slightly decrease for the $a_{\bullet} = 0.998$ run.

We also note that the $a_{\bullet} = 0.9375$ and $a_{\bullet} = 0.998$ runs had a standard deviation for accretion rate of 7.121 and 8.685 respectively. This indicates that the near-maximal case has more variable accretion rate, which is important as that is expected to also produce high total intensity variability. Currently, within the EHT collaboration, we are finding that most models, including that 0.9375 model, overestimates the variability of Sgr A* when compared to observations, and so noting that the near-maximal case only further increases variability indicates that it is not as likely of a candidate for Sgr A*.

We note the prevalence of "flux eruption events" as well within both simulations. Flux eruption events are noted as periods of sharp decrease in accretion rate and correspond to magnetic field reconnection releasing large amounts of magnetic energy into the plasma, pushing material in the disk away from the black hole. We see such events occur at $\approx t = 7,000M$ for $a_{\bullet} = 0.9375$ and at $\approx t = 9,700M$ and $\approx t = 5,400M$ for $a_{\bullet} = 0.998$.

4.1.2. Magnetic Field

4.1.2.1. Magnetization The motion of plasma around a black hole naturally creates an electric field and consequently a magnetic field. Some of these magnetic field lines thread through the BH horizon and this magnetic flux may be measured both directly and via the magnetic flux parameter ϕ_{BH} . ϕ_{BH} is a dimensionless quantity, calculated using the equation below [11, 31].

$$\phi_{BH}(t) = \frac{\sqrt{4\pi}}{2\sqrt{\dot{M}_0(t)}} \int_{\theta} \int_{\phi} |B^r|_{r=r_H} \sqrt{-g} d\theta d\phi \quad (13)$$

where the $\sqrt{4\pi}$ term converts the magnetic field strength B^r from Heaviside-Lorentz units to Gaussian units, \dot{M}_0 is the rest mass inflow rate through the disk as a function of time, g is the determinant of the metric, and r_H is the event horizon radius.

Using pyharm, ϕ_{BH} is tracked as a function of time, with the \dot{M}_0 being measured at $r = r_H \pm 0.01M$. Additionally, the following equation predicts the ϕ_{BH} as a function of spin based on previous GRMHD runs [11, 32].

$$\phi_{BH} = -20.2a_{\bullet}^3 - 14.9a_{\bullet}^2 + 34a_{\bullet} + 52.6 \quad (14)$$

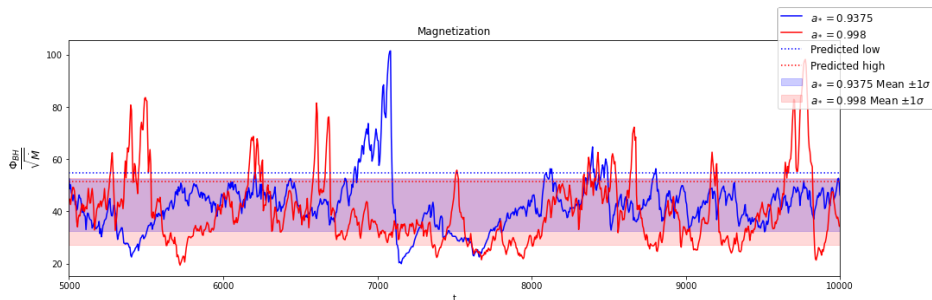


Figure 6. The magnetization as a function of time is shown for both $a_{\bullet} = 0.9375$ (blue) and $a_{\bullet} = 0.998$ (red). Additionally, the dashed horizontal lines reflect the predicted magnetization based on Tchekhovskoy et al. (2012) [11, 32]. For $a_{\bullet} = 0.9375$ and $a_{\bullet} = 0.998$ these values are ~ 54.735 and ~ 51.612 respectively. The highlighted blue and red regions show the mean of magnetization $\pm 1\sigma$ for $a_{\bullet} = 0.9375$ and 0.998 respectively.

The average ϕ_{BH} for $a_{\bullet} = 0.9375$ versus $a_{\bullet} = 0.998$ is ~ 45.25 and ~ 41.17 respectively which differs from the predicted ~ 54.735 and ~ 51.612 .

One possible reason for the predicted values being higher in both spin cases is that the equation 14 was based on GRMHD runs using an adiabatic index $\hat{\gamma} = \frac{5}{3}$ [11, 32]. Our lower $\hat{\gamma}$ of $\frac{13}{9}$ then may contribute to the lower than expected magnetization values.

That being said it's still important to note that our simulations seem to confirm that ϕ_{BH} decreases with increasing spin.

Additionally, we see that the $a_{\bullet} = 0.998$ run has very high variability in ϕ_{BH} . This, paired with the presence of dips in accretion rate, seem to suggest that for near-maximal spin it may take a longer time for the black hole to reach an equilibrium between the inward pressure from the accreting material and the outward magnetic pressure. Physically, this may be the source of quasi-periodic dips in accretion rate of varying intensities like what we see in the KHARMA density snapshots shown below.

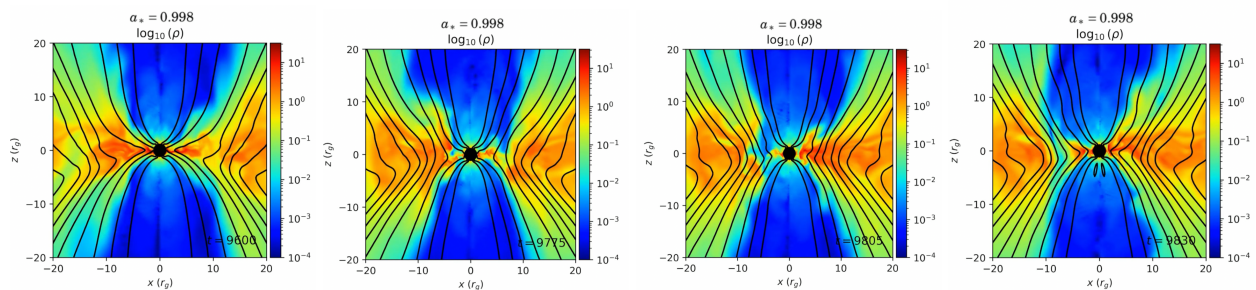


Figure 7. Density plots of the KHARMA GRMHD $a_{\bullet} = 0.998$ run during dips in accretion rate which roughly follow local peaks in ϕ_{BH} taken at $t = 9,600, 9,775, 9,805,$ and $9,830M$ from left to right.

Further time evolution of this simulation will be needed in order to see if these trends continue or if the BH does eventually reach some equilibrium state.

4.1.3. Jet Power

As discussed previously, under the Blandford-Znajek mechanism it is expected that as spin increases, so too will jet power and that the jet power output may even overcome the energy gained via accretion.

We can analyze this within GRMHD and particularly we look at the jet power efficiency as defined by equation 3. This power efficiency can be compared between different spins and also can be compared to the analytic approximation from equation 4. We measure the jet power and accretion rate at $r = 5M$.

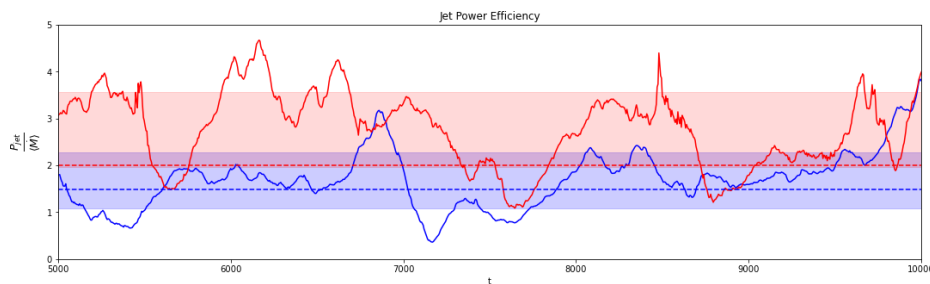


Figure 8. This plot shows the jet power efficiencies of $a_{\bullet} = 0.9375$ (blue) and $a_{\bullet} = 0.998$ (red) as a function of time. Additionally, the dashed horizontal lines reflect the predicted jet power based on equation 4 from Tchekhovskoy et al. (2010) [19]. The highlighted red and blue sections correspond to the mean jet power efficiency $\pm 1\sigma$ for $a_{\bullet} = 0.9375$ and 0.998 respectively.

From the graph above we note that our jet power efficiency is, on average, somewhat larger than predicted for both the $a_{\bullet} = 0.9375$ and $a_{\bullet} = 0.998$ case. In particular, for the near-maximal case, the jet power efficiency is much larger than predicted.

Considering the time averages directly lets us compare to the function proposed of average η as a function of spin found in Narayan et al. (2022) [11]. Narayan et al.'s setup means that the predicted curve technically is posed as some function $\eta(\phi_B)$ where ϕ_B is also a predicted magnetization curve fit to their simulations.

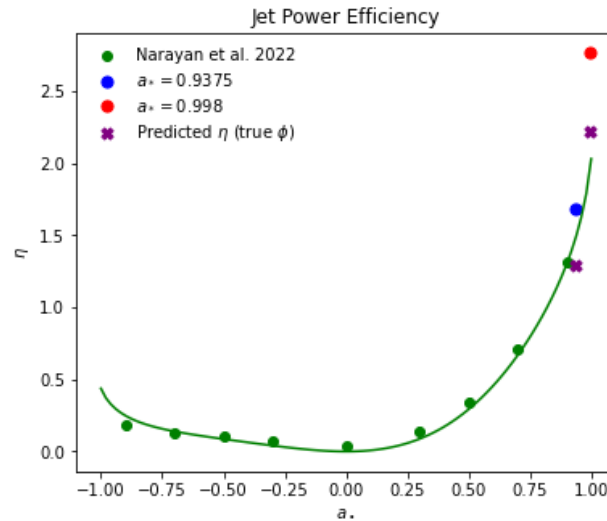


Figure 9. Above is a plot showing the jet power efficiency as a function of spin. Green indicates previously calculated values and the predicted curve [11]. The blue and red dots indicate our observed average jet power efficiency. The purple crosses indicate the predicted efficiency based on the true values for magnetization [19].

In the figure above we again see that the average jet power efficiency for our simulations is noticeably higher than predicted. Going forward we will continue to run our GRMHD simulations for a longer period of time to see if this trend continues or if there's some other aspect that is contributing to the high efficiency.

Since the jet extracts rotational energy from the black hole, we also expect it to significantly impact the spin and we can track this impact with the spin-up parameter introduced in equation 5. Note that the spin-up values shown in the graph below were taken at $r = 5M$.

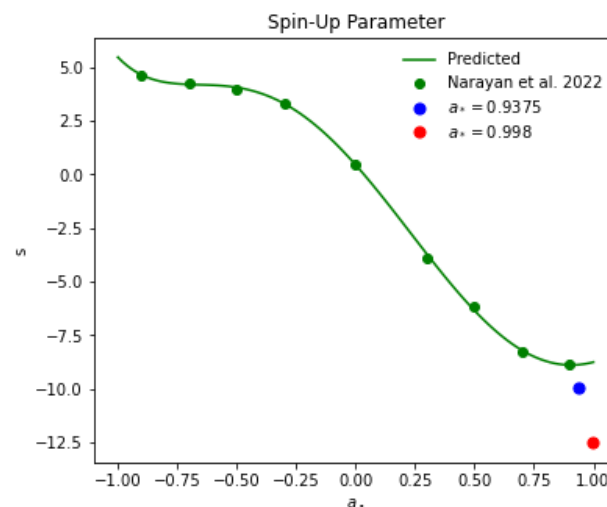


Figure 10. Above is a plot of the spin-up parameter as a function of spin. Green indicates previously calculated values and the predicted curve [11]. The blue and red dots indicate our observed average spin-up parameter.

As seen above, the spin-up parameter is more significantly negative for the 0.9375 and 0.998 runs. This corresponds to a more intense and rapid spin-down of the black hole by its incredibly powerful jet.

4.2. Observable Signatures

In order to approximate the EHT's observational capabilities we apply a Gaussian blur to images produced such that they have a final resolution of $20\mu\text{as}$. This shall be the default resolution for all figures and analysis unless otherwise specified.

Additionally, R_{high} is a parameter which helps control electron temperature and specifically, as R_{high} is increased the electrons become cooler which can significantly impact the flux and faraday rotation depth [33]. For the runs discussed in this paper we use an $R_{high} = 160$, but plan to explore more values of it soon.

4.2.1. Image Differences

Using IPOLE we created movies for the $a_{\bullet} = 0.998$ and $a_{\bullet} = 0.9375$ runs over the course of $t = 5,000 - 10,000M$.

The videos aren't directly comparable frame by frame since the variability is driven by random instantiations of the turbulence. That being said we are able to evaluate trends over time by evaluating the light curve shown below.

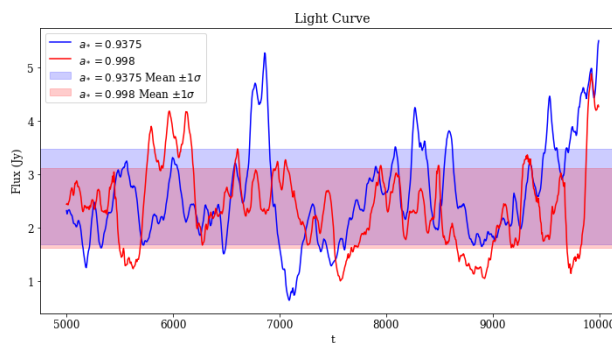


Figure 11. Above is the light curve of total flux for our $a_{\bullet} = 0.998$ and $a_{\bullet} = 0.9375$ runs.

By eye, the light curves between the two spins exhibit similar variability amplitudes and timescales.

Aside from the light curve, we can also examine the overall image differences by taking an average over the full time span.

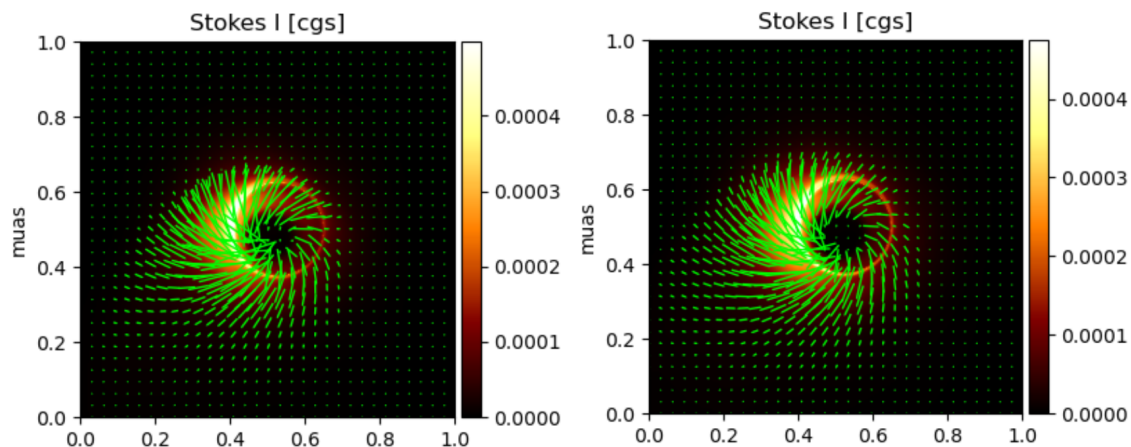


Figure 12. Above are the time averaged images for the $a_{\bullet} = 0.998$ (left) and $a_{\bullet} = 0.9375$ runs (right). The average is taken over the course of 5,000-10,000M and involves averaging all stokes parameters.

Looking at the average images shown above, there appears to be slightly more intense linear polarization from the inner region near the black hole for the $a_{\bullet} = 0.998$ case. However, the overall region in which we see considerable linear polarization is also slightly smaller for the $a_{\bullet} = 0.998$ case. This can be more clearly seen in the following images of the averaged linear polarization fraction.

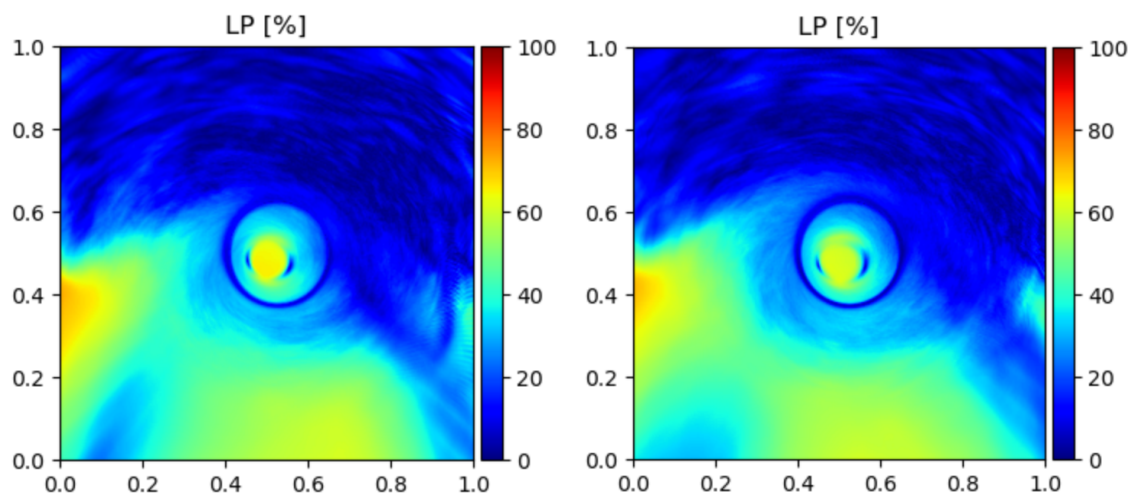


Figure 13. Above are the time averaged images of linear polarization for the $a_{\bullet} = 0.998$ (left) and $a_{\bullet} = 0.9375$ runs (right). The average is taken over the course of 5,000-10,000M.

This trend fits with the expectation of higher spins producing more tightly wound magnetic field lines due to frame dragging. The effect of spin on average polarization morphology is incredibly subtle and only becomes noticeable with a sufficient number of observations over which to average. While the effects noted here may not currently be observationally accessible, in the future, with higher resolution and a potential "movie" of M87*, this may serve as a way to roughly constrain spin.

4.2.2. Polarization

Within the IPOLE images we are also able to examine polarization. This is a key aspect of the images as most of the emission EHT detects comes from synchrotron radiation which occurs when relativistic charged particles are rotated around magnetic field lines. The resulting radiation is polarized perpendicular to the

magnetic field projected onto the sky, and so by determining linear polarization you can probe the magnetic field structure of a black hole.

Below is a list of the most relevant polarization metrics, which I describe in more detail below.

- m_{net}
- v_{net}
- Phase and magnitude of β_2

4.2.2.1. m_{net} The spatially unresolved linear polarization fraction, obtainable by e.g., a single-dish measurement of a source. This is calculated via.

$$m_{net} = \frac{\sqrt{(\sum_{pixel} Q)^2 + (\sum_{pixel} U)^2}}{\sum_{pixel} I} \quad (15)$$

where I , Q , and U are the Stokes parameters.

4.2.2.2. v_{net} The analogous quantity for circular polarization, calculated via

$$v_{net} = \frac{\sum_{pixel} V}{\sum_{pixel} I} \quad (16)$$

Small amounts of circular polarization naturally occur as part of synchrotron radiation, however the primary source of circular polarization within EHT images would be due to Faraday conversion [EHTC+2023, 34]. Essentially, as linearly polarized light propagates along its wavevector, one of two mechanisms convert Q to U which then can be Faraday converted into circular polarization [34].

v_{net} specifically helps inform the direction of the poloidal field in the observer's line of sight [33].

4.2.2.3. β_2 β_2 is a 2nd mode decomposition coefficient defined by the equation below [35].

$$\beta_2 = \frac{1}{I_{ann}} \int_{\rho_{min}}^{\rho_{max}} \int_0^{2\pi} P(\rho, \varphi) e^{-i2\varphi} \rho d\varphi d\rho \quad (17)$$

where I_{ann} is the total Stokes I flux in the annulus, ρ_{min} and ρ_{max} are the radial extent of the annulus, and $P(\rho, \varphi)$ is the complex valued polarization field $Q(\rho, \varphi) + iU(\rho, \varphi)$.

In a simpler sense, β_2 is a complex number that summarizes the rotationally-symmetric structure of linear polarization ticks. The phase encodes the pitch angle, while the magnitude encodes the strength of this mode[35]. This can be best visualized with the graphic below from Figure 1 in Palumbo et al. (2020) [35].

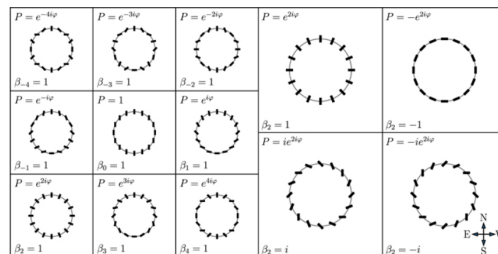


Figure 14. An illustration of polarization ticks and the corresponding β modes 1-4 from Palumbo et al. (2020), along with an depiction of polarization ticks and the corresponding phases for β_2 [35].

Because the underlying magnetic field structure is rotationally symmetric, numerous studies have demonstrated that β_2 is a sensitive tracer of spin (?). Thus, it is of interest how rapidly this observable changes between our two spin values.

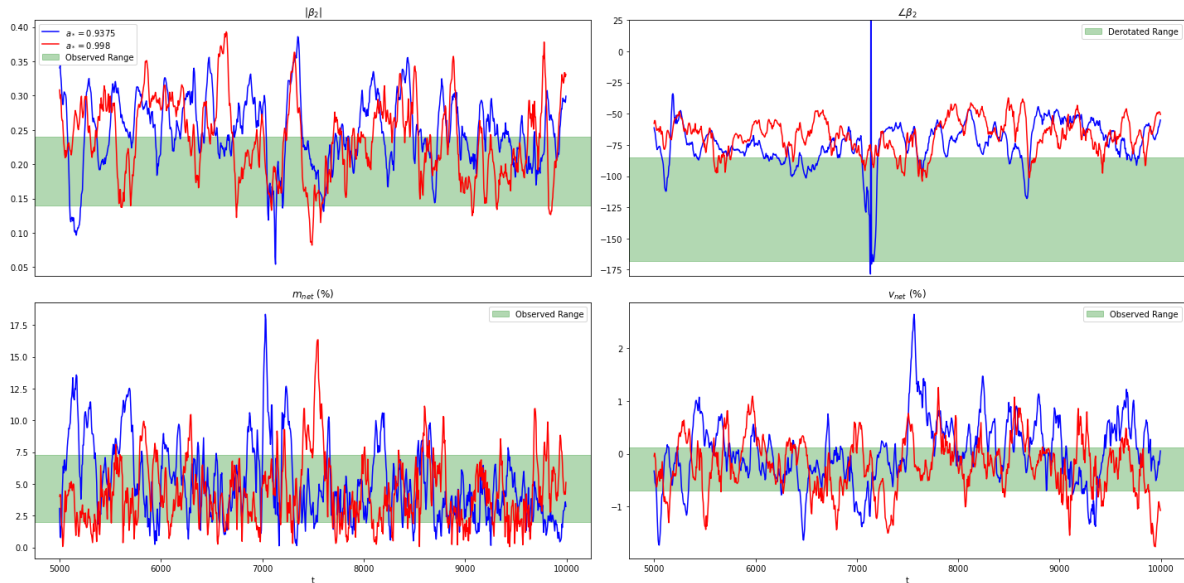


Figure 15. Above are 4 plots showing the magnitude and argument of β_2 (top left and top right) as well as the linear and circular polarization fraction (bottom left and bottom right). The blue indicates our $a_\bullet = 0.9375$ run while red indicates the 0.998 run. The green shows the observationally constrained values for Sgr A* according to the EHT [33].

4.2.2.4. Polarimetric Results Above we note very similar values for almost all of our polarimetric quantities between the 0.998 and 0.9375 runs. Both spin values seem to fit well with Sgr A* constraints for all metrics, although the agreement with $\angle\beta_2$ is marginal. This is fully consistent with previous studies (?). We report no significant difference in these polarized metrics between $a_\bullet = 0.9375$ and $a_\bullet = 0.998$, suggesting that EHT observations of Sgr A* are at present consistent with a $a_\bullet = 0.998$ black hole.

4.2.3. $n=1$ Photon Ring

One of the key scientific goals of ngEHT alongside BHEX is to resolve the $n=1$ photon ring [6]. For that reason, it's important to check the observability in differences of the photon ring between $a_\bullet = 0.998$ and $a_\bullet = 0.9375$.

As seen in figure 2, the most intense effects to the critical curve, and therefore the photon ring, occurs when the black hole is viewed at an inclination of 90° . For our photon ring I therefore focused on this inclination, however with a 90° inclination the treatment of what is included as part of the photon ring within our code gets a bit wonky. Specifically, IPOLE determines each subring by continuously checking if a photon has reached or crossed the midplane. This becomes an issue when $i = 90^\circ$ because then nearly all of the photons are included as having passed the midplane in order to be included in the image and didn't truly orbit the black hole and therefore don't tell us nearly as much information. In this way when looking perfectly edge on, the line between the $n=0$ and $n=1$ rings get confusing and instead we look at what the code considers the $n=2$ ring, but what truly includes mostly photons that have undergone 1.5 orbits. For simplicity's sake, we will refer to this simply as the $n=1$ photon ring.

We image this for both of our spin values and can overlay the two images to note differences, which is shown below.

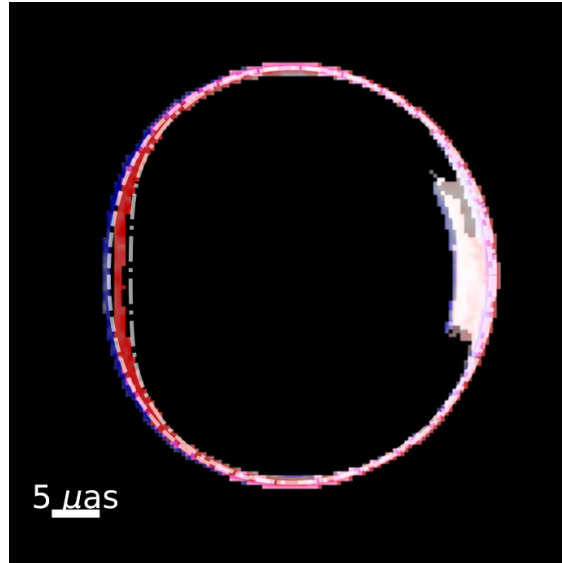


Figure 16. Overlapped IPOLE images of the $n=1$ photon ring taken with a resolution of $0\mu\text{as}$ for the $a_{\bullet} = 0.9375$ (blue) and $a_{\bullet} = 0.998$ (red) case. The dashed lines correlate to the $n=\infty$ rings for $a_{\bullet} = 0.9375$ (white dashed curve) and $a_{\bullet} = 0.998$ (white dashed and dotted curve).

We note that there's a visible distortion of the photon ring for the $a_{\bullet} = 0.998$ case. This distortion is subtle and is approximately of order of a few μas , so further work will be need to be done to determine if it would be resolvable with future ngEHT and BHEX resolution.

Additionally, we can note that the simulated distortion is only slightly less prominent than the expected distortion of the $n=\infty$ ring. This is consistent with theoretical expectations since the $n = 1$ ring is not entirely insensitive to the $n = 0$ emission profile. However, it's important to note that as n increases the corresponding rings become exponentially fainter. Only the $n = 1$ will be resolvable using BHEX, with $n > 1$ requiring telescopes as distant as the moon. Having access to only $n = 1$, we have demonstrated that fitting this curve with an $n = \infty$ template would lead to an under-estimate of the spin.

5. CONCLUSION

In summary, we have found that

1. $a_{\bullet} = 0.998$ models show similar accretion rates & magnetization as their $a_{\bullet} = 0.9375$ counterparts
2. Jet efficiency increases more than expected for $a_{\bullet} = 0.998$, and spin-up also deviates from previous predictions.
3. The observable polarimetric quantities of $a_{\bullet} = 0.998$ and 0.9375 models are very similar, and roughly agree with current Sgr A* EHT observations.
4. At high resolution, near-maximal spin results in a visible distortion of the photon ring image.

So far, both the $a_{\bullet} = 0.998$ and $a_{\bullet} = 0.9375$ match existing constraints on Sgr A*, but additional constraints will be considered, including time variability. In our results so far, the jet efficiency is the most promising way to discriminate between these two spin values, although this is difficult to access observationally.

As extensions to the EHT are developed both on land, with the next-generation EHT project, and in space, with the Black Hole Explorer mission, signatures of near-maximal spin may become observationally accessible via the photon ring.

Our results regarding the spin-up parameter and jet power efficiency would suggest faster than expected spin-down of SMBHs over cosmological timescales. Depending on accretion rate, this could significantly influence AGN feedback and could help us better model galaxy evolution.

One main limitation of our research so far is that we have only run simulations out to $10,000t_g$, in comparison to the $100,000t_g$ used in similar papers [11]. Going forward, we plan on extending our simulations, which will help ensure greater confidence in the stability and significance of our results. Additionally, this will allow us to better compare model variability to Sgr A*.

ACKNOWLEDGEMENTS

Thank you to the National Society of Black Physicists, the Smithsonian Astrophysical Observatory, and the Event Horizon Telescope Collaboration. Many thanks as well to Daniel Palumbo and Richard Anantua.

This work was supported by the Gordon and Betty Moore Foundation (Grant GBMF-10423).

References

- ¹Event Horizon Telescope Collaboration et al., “First M87 Event Horizon Telescope Results. I. The Shadow of the Supermassive Black Hole”, [ApJ 875, L1, L1 \(2019\)](#).
- ²Event Horizon Telescope Collaboration et al., “First Sagittarius A* Event Horizon Telescope Results. I. The Shadow of the Supermassive Black Hole in the Center of the Milky Way”, [ApJ 930, L12, L12 \(2022\)](#).
- ³Event Horizon Telescope Collaboration et al., “First Sagittarius A* Event Horizon Telescope Results. VII. Polarization of the Ring”, [ApJ 964, L25, L25 \(2024\)](#).
- ⁴Event Horizon Telescope Collaboration et al., “First M87 Event Horizon Telescope Results. VII. Polarization of the Ring”, [ApJ 910, L12, L12 \(2021\)](#).
- ⁵M. D. Johnson et al., “Key Science Goals for the Next-Generation Event Horizon Telescope”, [Galaxies 11, 61, 61 \(2023\)](#).
- ⁶M. Johnson et al., “The black hole explorer: motivation and vision”, in [Space telescopes and instrumentation 2024: optical, infrared, and millimeter wave](#), edited by L. E. Coyle, M. D. Perrin, and S. Matsuura (Aug. 2024), p. 90.
- ⁷Event Horizon Telescope Collaboration et al., “First M87 Event Horizon Telescope Results. V. Physical Origin of the Asymmetric Ring”, [ApJ 875, L5, L5 \(2019\)](#).
- ⁸K. S. Thorne, “Disk-Accretion onto a Black Hole. II. Evolution of the Hole”, [ApJ 191, 507–520 \(1974\)](#).
- ⁹C. F. Gammie, S. L. Shapiro, and J. C. McKinney, “Black Hole Spin Evolution”, [ApJ 602, 312–319 \(2004\)](#).
- ¹⁰S. L. Shapiro, “Spin, Accretion, and the Cosmological Growth of Supermassive Black Holes”, [ApJ 620, 59–68 \(2005\)](#).
- ¹¹R. Narayan et al., “Jets in magnetically arrested hot accretion flows: geometry, power, and black hole spin-down”, [MNRAS 511, 3795–3813 \(2022\)](#).
- ¹²A. Ricarte, R. Narayan, and B. Curd, “Recipes for Jet Feedback and Spin Evolution of Black Holes with Strongly Magnetized Super-Eddington Accretion Disks”, [ApJ 954, L22, L22 \(2023\)](#).
- ¹³B. Lowell et al., “Rapid Black Hole Spin-down by Thick Magnetically Arrested Disks”, [ApJ 960, 82, 82 \(2024\)](#).
- ¹⁴B. Lowell et al., “Evidence for Low Universal Equilibrium Black Hole Spin in Luminous Magnetically Arrested Disks”, [arXiv e-prints, arXiv:2502.17559, arXiv:2502.17559 \(2025\)](#).
- ¹⁵E. Berti and M. Volonteri, “Cosmological Black Hole Spin Evolution by Mergers and Accretion”, [ApJ 684, 822–828 \(2008\)](#).
- ¹⁶R. D. Blandford and R. L. Znajek, “Electromagnetic extraction of energy from Kerr black holes.”, [MNRAS 179, 433–456 \(1977\)](#).
- ¹⁷S. W. Davis and A. Tchekhovskoy, “Magnetohydrodynamics simulations of active galactic nucleus disks and jets”, [Annual Review of Astronomy and Astrophysics 58, 407–439 \(2020\)](#).
- ¹⁸A. Ricarte et al., “Multimessenger Probes of Supermassive Black Hole Spin Evolution”, [ApJ 980, 136, 136 \(2025\)](#).
- ¹⁹A. Tchekhovskoy, R. Narayan, and J. C. McKinney, “Black Hole Spin and The Radio Loud/Quiet Dichotomy of Active Galactic Nuclei”, [ApJ 711, 50–63 \(2010\)](#).

- ²⁰A. Chael, M. Johnson, and A. Lupsasca, “The Inner Shadow of the Black Hole in M87*: A Direct View of the Event Horizon”, in American astronomical society meeting #240, Vol. 240, American Astronomical Society Meeting Abstracts (June 2022), p. 432.08.
- ²¹The Event Horizon Telescope Collaboration, “First Sagittarius A* Event Horizon Telescope Results. V. Testing Astrophysical Models of the Galactic Center Black Hole”, [arXiv e-prints](#), [arXiv:2311.09478](#), [arXiv:2311.09478 \(2023\)](#).
- ²²D. C. M. Palumbo et al., “Demonstrating Photon Ring Existence with Single-baseline Polarimetry”, [ApJ](#) **952**, L31, L31 (2023).
- ²³A. Ricarte et al., “The ngEHT’s Role in Measuring Supermassive Black Hole Spins”, [Galaxies](#) **11**, 6, 6 (2023).
- ²⁴A. Chael, M. D. Johnson, and A. Lupsasca, “Observing the Inner Shadow of a Black Hole: A Direct View of the Event Horizon”, [ApJ](#) **918**, 6, 6 (2021).
- ²⁵G. N. Wong et al., “PATOKA: Simulating Electromagnetic Observables of Black Hole Accretion”, [ApJS](#) **259**, 64, 64 (2022).
- ²⁶L. G. Fishbone and V. Moncrief, “Relativistic fluid disks in orbit around Kerr black holes.”, [ApJ](#) **207**, 962–976 (1976).
- ²⁷A. Mignone and J. C. McKinney, “Equation of state in relativistic magnetohydrodynamics: variable versus constant adiabatic index”, [MNRAS](#) **378**, 1118–1130 (2007).
- ²⁸R. Narayan, I. V. Igumenshchev, and M. A. Abramowicz, “Magnetically Arrested Disk: an Energetically Efficient Accretion Flow”, [PASJ](#) **55**, L69–L72 (2003).
- ²⁹R. Narayan et al., “GRMHD simulations of magnetized advection-dominated accretion on a non-spinning black hole: role of outflows”, [MNRAS](#) **426**, 3241–3259 (2012).
- ³⁰M. Mościbrodzka and C. F. Gammie, “IPOLE - semi-analytic scheme for relativistic polarized radiative transport”, [MNRAS](#) **475**, 43–54 (2018).
- ³¹A. Tchekhovskoy, R. Narayan, and J. C. McKinney, “Efficient generation of jets from magnetically arrested accretion on a rapidly spinning black hole”, [MNRAS](#) **418**, L79–L83 (2011).
- ³²A. Tchekhovskoy, J. McKinney, and R. Narayan, *Journal of physics conference series*, 2012.
- ³³Event Horizon Telescope Collaboration et al., “First Sagittarius A* Event Horizon Telescope Results. VIII. Physical Interpretation of the Polarized Ring”, [ApJ](#) **964**, L26, L26 (2024).
- ³⁴A. Ricarte, R. Qiu, and R. Narayan, “Black hole magnetic fields and their imprint on circular polarization images”, [MNRAS](#) **505**, 523–539 (2021).
- ³⁵D. C. M. Palumbo, G. N. Wong, and B. S. Prather, “Discriminating Accretion States via Rotational Symmetry in Simulated Polarimetric Images of M87”, [ApJ](#) **894**, 156, 156 (2020).

This paper has been typeset from a $\text{\TeX}/\text{\LaTeX}$ file prepared by the author.